

# The simulation of molecular clouds formation in the Milky Way

S.A. Khoperskov,<sup>1</sup> E.O. Vasiliev,<sup>2</sup> A.M. Sobolev,<sup>3</sup> A.V. Khoperskov<sup>4</sup>

<sup>1</sup>*Institute of Astronomy Russian Academy of Sciences, Pyatnitskaya st., 48, 119017, Moscow, Russia*

<sup>2</sup>*Institute of Physics, Department of Physics, Southern Federal University, Stachki Ave. 194, 344090 Rostov-on-Don, Russia*

<sup>3</sup>*Ural Federal University, Lenin ave. 51, Ekaterinburg 620000, Russia*

<sup>4</sup>*Volgograd State University, Universitetskiy pr., 100, Volgograd 400062, Russia*

Accepted 3004 December 15. Received 2004 December 14; in original form 2004 December 31

## ABSTRACT

Using 3D hydrodynamic calculations we simulate formation of molecular clouds in the Galaxy. The simulations take into account molecular hydrogen chemical kinetics, cooling and heating processes. Comprehensive gravitational potential accounts for contributions from the stellar bulge, two and four armed spiral structure, stellar disk, dark halo and takes into account self-gravitation of the gaseous component. Gas clouds in our model form in the spiral arms due to shear and wiggle instabilities and turn into molecular clouds after  $t \gtrsim 100$  Myr. At the times  $t \sim 100 - 300$  Myr the clouds form hierarchical structures and agglomerations with the sizes of 100 pc and greater. We analyze physical properties of the simulated clouds and find that synthetic statistical distributions like mass spectrum, "mass-size" relation and velocity dispersion are close to those observed in the Galaxy. The synthetic  $l - v$  (galactic longitude - radial velocity) diagram of the simulated molecular gas distribution resembles observed one and displays a structure with appearance similar to Molecular Ring of the Galaxy. Existence of this structure in our modelling can be explained by superposition of emission from the galactic bar and the spiral arms at  $\sim 3-4$  kpc.

**Key words:** galaxies: ISM — Galaxy: structure — ISM: clouds

## 1 INTRODUCTION

Molecular clouds represent one of the major constituents of our galaxy (Dame *et al.* 2001). Their masses and sizes vary in a wide range (e.g. Solomon *et al.* 1987). Molecular clouds play very important role in determination of the structure and evolution of the Galaxy. This can be illustrated by the fact that the stars and their clusters originate from molecular clouds (Shu *et al.* 1987; McKee & Ostriker 2007; Lada & Lada 2003). The dynamical time of disintegration for molecular clouds in the Milky Way is much shorter than the rotation period of the galaxy (e.g. Blitz & Shu 1980). So, explanation of the observational fact of existence of the rich population of molecular clouds requires involvement of efficient mechanisms leading to formation of molecular clouds in the Galaxy. Special interest is paid to formation of the giant molecular clouds (GMC) which have masses  $\gtrsim 10^6 M_\odot$  (Dame *et al.* 1986). Two main theories of the GMC formation were proposed. The first one explains formation of the GMCs by large scale magnetic and/or gravitational instabilities (Elmegreen 1979; Balbus & Cowie 1985; Elmegreen 1994; Chou *et al.* 2000; Kim & Ostriker 2006). In the second one the GMCs are built up by coalescence of the smaller molecular clouds (Field & Saslaw 1965; Levinson

& Roberts 1981; Tomisaka 1984; Roberts & Stewart 1987; Kwan & Valdes 1987) or interaction of the turbulent flows (e.g. Ballesteros-Paredes *et al.* 2007). In reality both types of processes are expected to play significant role (Zhang & Song 1999; Dobbs 2008).

Large scale perturbations in a gas of the Galactic disk can be generated not only by magnetic fields or self-gravity, but also by the galactic spiral shock wave (Roberts 1969; Nelson & Matsuda 1977). A simple analysis of the global galactic shock wave shows that such shocks are unstable (Mishurov & Suchkov 1975). Obviously, large scale shear flows in the Galactic shocks lead to the development of both wiggle and Kelvin-Helmholz instabilities (Wada 2001; Wada & Koda 2004). Such hydrodynamic instabilities are expected to give a birth to spurs, gaseous fragments and turbulent flows (Wada 1994; Wada *et al.* 2000; Dobbs & Bonnel 2006; Shetty & Ostriker 2006). The gravitational and thermal (in general, thermo-chemical) instabilities are expected to develop further fragmentation, which leads to formation of the population of molecular clouds.

The properties of molecular clouds (mass, size, density, temperature etc.) are intensively studied both observationally (Solomon *et al.* 1987; Falgarone *et al.* 1992; Lada *et al.*

2008; Heyer *et al.* 2009; Rathborne *et al.* 2009; Kauffmann *et al.* 2010; Román-Zúñiga *et al.* 2010) and numerically (Dobbs *et al.* 2006; Dobbs & Bonnell 2007a,b; Tasker & Tan 2009; Glover & Mac Low 2011). Efforts in order to understand dependencies between physical parameters of the clouds lead to establishment of several empirical relationships for the properties of molecular clouds (Larson 1981). In particular, the mass-size relation reflects the hierarchical spatial structure of clouds (Beaumont *et al.* 2012). Molecular clouds can agglomerate in small groups and chains, thus reflecting processes of the cloud formation: disintegration into smaller clumps or combining into bigger clouds. Due to the origin of the clouds from the large scale perturbations in the galactic disk molecular clouds can trace the large-scale structures, e.g. spiral arms and the bar (e.g. Wada & Koda 2004). Several observational studies display existence of the galactic molecular ring (Stecker *et al.* 1975; Cohen & Thaddeus 1977; Roman-Duval *et al.* 2010), however it is unclear whether this is an actual ring or just superposition of emission from molecular clouds belonging to different spiral arms (Dobbs & Burkert 2012).

In this paper we develop a model aiming to reproduce general characteristics of the formation of molecular clouds in the Galaxy, their physical properties, their distribution in the Milky Way using the 3D simulations with the comprehensive gravitational potential, self-gravity of gaseous component, molecular hydrogen chemical kinetics, cooling and heating processes.

The paper is organized as follows. Section 2 describes basic premises and equations of our model. Section 3 presents numerical results on the disk evolution. Section 4 presents analysis of the physical properties of the clouds in our model. Section 5 considers large-scale structures in the simulated Galaxy. Section 6 summarizes the results.

## 2 MODEL

### 2.1 Gas dynamics and galaxy potential

The dynamics of the chemically reacting gas mixture in our model of the Galaxy can be written in the single-fluid approximation as follows:

$$\frac{\partial \rho}{\partial t} + \nabla \cdot (\rho \mathbf{u}) = 0, \quad (1)$$

$$\frac{\partial \rho \chi_i}{\partial t} + \nabla \cdot (\rho \mathbf{u} \chi_i) = \rho s_i, \quad i = 1, \dots, n_s, \quad (2)$$

$$\frac{\partial \mathbf{u}}{\partial t} + \nabla \cdot (\mathbf{u} \otimes \mathbf{u}) = -\frac{\nabla p}{\rho} - \nabla (\Psi_{ext} + \Psi_g), \quad (3)$$

$$\frac{\partial E}{\partial t} + \nabla \cdot ([E + p] \mathbf{u}) = -\mathbf{u} \cdot \nabla (\Psi_{ext} + \Psi_g) - (\Lambda - \Gamma), \quad (4)$$

where  $\rho$  is the gas density,  $p$  is the gas pressure,  $\mathbf{u} = (u, v, w)$  is the gas velocity vector,  $n_s$  is the number of components in the gas mixture (in our model  $n_s = 2$ ),  $\chi_i = \rho_i / \rho$  is the mass fraction of  $i$ -th component of gas,  $\sum_{i=1}^{n_s} \chi_i = 1$ ,  $s_i$  is the formation/destruction rate of  $i$ -th component,  $E = \rho(e + \frac{\mathbf{u}^2}{2})$  is the total energy,  $e$  is the specific internal energy,  $\Lambda$  and  $\Gamma$  are the cooling and heating rates, correspondingly,  $\Psi_g$  is the gravitational potential of gas,  $\Psi_{ext}$  is the total external

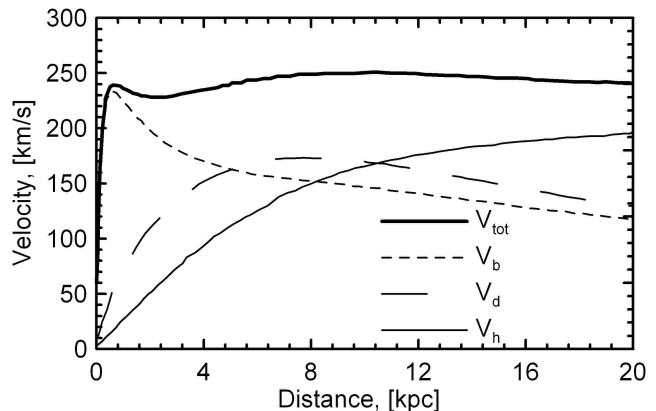


**Figure 1.** The rotation curve of the gas components in our model of the Galaxy,  $V_{tot}$  (thick solid line). The contributions from the stellar bulge,  $V_b$ , the stellar disk,  $V_d$ , and the dark halo,  $V_h(r)$ , are shown by dash, long dash and thin solid lines, correspondingly.

gravitational potential produced by the massive dark halo  $\Psi_{halo}$ , the stellar bulge  $\Psi_{bulge}$  and the stellar disk  $\Psi_{disk}$ . The latter includes the potentials of the spiral structure and the bar. The potential of the gaseous component is determined by the Poisson equation:

$$\Delta \Psi_g = 4\pi G \rho. \quad (5)$$

Hereafter we assume  $G = 1$ . The external gravitational potential can be written as follows:

$$\Psi_{ext} = \Psi_{halo} + \Psi_{bulge} + \Psi_{disk}. \quad (6)$$

Figure 1 present the rotation curve of the gas components adopted in our model of the Galaxy. For the maximum rotation velocity of the Milky Way we adopt a value obtained from the analysis of the recent observational data on the Galactic masers (Bobylev & Bajkova 2010). The external gravitational potential of the Galactic subsystems, e.g. stellar bulge, stellar disk and dark halo,  $\Phi_{ext}$ , produces this rotation curve with the parameters for the Galactic subsystems fitted by Khoperskov & Tiurina (2003). The detailed description of the gravitational potential components is given in Appendix.

In our calculations we use the value of the angular velocity  $\Omega_p = 31 \text{ km s}^{-1} \text{ pc}^{-2}$  as a fiducial value. This value is realized at the radius of corotation  $R_c \sim 8 \text{ kpc}$  (Bobylev & Bajkova 2010). Our simulations have shown that variation of  $\Omega_p$  in the range  $18 - 28 \text{ km s}^{-1} \text{ pc}^{-2}$  (Amores *et al.* 2009; Sofue *et al.* 2009; Lepine *et al.* 2001) does not produce significant changes in the general properties of evolution of gas in the simulated Galaxy.

### 2.2 Chemical kinetics

$\text{H}_2$  molecules in the interstellar medium are formed on the surface of the dust grains and dissociated by ultraviolet Lyman-Werner photons and cosmic rays. We suppose that the dust density is proportional to the gas density because the dust is well mixed with gas on the scales of our simulations. Thus, evolution of molecular hydrogen number density can be found from (Bergin *et al.* 2004)

$$\frac{dn_2}{dt} = R_{gr}(T)n_1n - [\zeta_{cr} + \zeta_{diss}(N_2, A_V)]n_2, \quad (7)$$

where  $n_1, n_2$  are the number densities of atomic and molecular hydrogen, correspondingly,  $n = n_1 + 2n_2$  is the total number density of hydrogen species,  $N_2$  is the  $H_2$  column density,  $R_{gr}(T) = 2.2 \times 10^{-18} ST^{0.5}$  is the  $H_2$  formation rate on dust grains (Tielens & Hollenbach 1985),  $S = 0.3$  is the efficiency of the  $H_2$  formation on dust (Cazaux & Tielens 2004),  $\zeta_{cr} = 6 \times 10^{-18} \text{ s}^{-1}$  is the cosmic ray ionization rate,  $A_V$  is the extinction. Following Draine & Bertoldi (1996) the photodissociation rate can be estimated as:

$$\zeta_{diss}(N(H_2), A_V) = \zeta_{diss}(0) f_{shield}(N(H_2)) f_{dust}, \quad (8)$$

where  $\zeta_{diss}(0) = 4.17 \times 10^{-11} \text{ sec}^{-1}$  is the unshielded photodissociation rate,  $f_{shield}(N(H_2))$  is the  $H_2$  self-shielding factor,  $f_{dust}$  is the dust absorption factor.

To calculate the factors  $f_{shield}$  and  $f_{dust}$  we need to know both molecular,  $N(H_2)$ , and total,  $N_{tot} = N(HI) + 2N(H_2)$ , hydrogen column densities. In order to do this accurately we should find a cumulative ultraviolet radiation field produced by the young stars and their clusters. Obviously, this problem is extremely complex, moreover, star formation processes are not included in our model. Hence, we follow a simplified approach introduced by Dobbs (2008). We use a simple estimate that the column densities of the chemical species are just the local densities of these species multiplied by the typical distance to a young star,  $l_{ph}$ :  $N(HI, H_2) = l_{ph} \cdot n(HI, H_2)$ . This distance is assumed to be a constant length scale for the whole disk. In our simulations we take  $l_{ph} = 30 \text{ pc}$ , which is in agreement with the number of massive stars expected from the Salpeter initial mass function.

We assume that the Galactic gas has solar metallicity with the abundances given in Asplund *et al.* (2005):  $[C/H] = 2.45 \times 10^{-4}$ ,  $[O/H] = 4.57 \times 10^{-4}$ ,  $[Si/H] = 3.24 \times 10^{-5}$ . We assume that the dust depletion factors are equal to 0.72, 0.46 and 0.2 for C, O and Si, correspondingly. Chemical kinetics of the heavy elements is not solved in our model. We suppose that the carbon and silicon are singly ionized and oxygen stays neutral. This assumption is acceptable for the interstellar medium of the Milky Way due to existence of the strong ultraviolet radiation in the range  $\sim 10\text{-}13 \text{ eV}$  (Habing 1968).

### 2.3 Cooling and heating processes

The cooling rates are computed separately for the temperatures below and above  $2 \times 10^4 \text{ K}$ . In the low temperature range the cooling rate  $\Lambda$  in the energy equation (4) includes the typical processes of radiative losses for the interstellar medium: cooling due to recombination and collisional excitation and free-free emission of hydrogen (Cen 1992), molecular hydrogen cooling (Galli & Palla 1998), cooling in the fine structure and metastable transitions of carbon, oxygen and silicon (Hollenbach & McKee 1989), energy transfer in collisions with the dust particles (Wolfire *et al.* 2003) and recombination cooling on the dust (Bakes & Tielens 1994). In the high temperature range,  $T > 2 \times 10^4 \text{ K}$ , the cooling rate for solar metallicity is taken from Sutherland & Dopita (1993). We note that in our calculations the gas temperature is generally below  $10^4 \text{ K}$ , higher temperature is reached only in small rarefied regions at the periphery of the disk.

The heating rate  $\Gamma$  in the equation (4) takes into account photoelectric heating on the dust particles (Bakes &

Tielens 1994; Wolfire *et al.* 2003), heating due to  $H_2$  formation on the dust, and the  $H_2$  photodissociation (Hollenbach & McKee 1979) and the ionization heating by cosmic rays (Goldsmith *et al.* 1978).

### 2.4 Numerical methods

To solve the system of gas dynamical equations (1-4) we use nonlinear finite-volume numerical scheme TVD MUSCL in the Cartesian coordinates (van Leer 1979). The continuity equation for chemical species is constructed using the operator splitting scheme. Note that because in our model we have two chemical species, HI and  $H_2$ , we can solve the kinetics equation for one of them only, e.g. for  $H_2$ . At first we solve the continuity equation without right-hand terms and update the  $H_2$  density due to advection. Then we update this result after solution of chemical reactions. The equation for  $H_2$  (7) is integrated using a fourth-order Runge-Kutta method. To find the gravitational potential of the gas (5) we use the TreeCode method (Barnes & Hut 1986).

The numerical resolution is  $4096 \times 4096 \times 20$  cells. The cells are assumed to be cubic with the sides of 7.3 pc. Therefore, the physical size of the computational grid is  $30 \times 30 \times 0.15 \text{ kpc}$ . We also made calculations with higher resolution in the vertical direction, but lower in the disk plane direction, e.g.  $1024 \times 1024 \times 100$ , and did not find significant difference in global characteristics of gas evolution. We expect that this is sufficient to model the large scale dynamics of the Galactic disk and to study the formation of the spurs and molecular clouds in the vicinity of the spiral arms.

## 3 DISK EVOLUTION

Figure 2 shows the surface gas density at 50, 100, 200 and 300 Myr. At the beginning the spiral shocks are formed due to the supersonic gas flow through the spiral gravitational potential of the stellar disk. After  $t = 50 \text{ Myr}$  one finds a well-developed spiral structure in the gas disk (upper left panel). The width of the gas spirals is significantly smaller than that of the stellar density wave due to higher stellar velocity dispersion. Owing to shear and wiggle instabilities the shock front becomes perturbed, and as a result the spurs and fragments are formed. Such spurs and fragments can be found at  $t = 50 \text{ Myr}$  (upper left panel) and are clearly seen at  $t = 100 \text{ Myr}$  (upper right panel). On one hand, higher density in such fragments stimulates molecular hydrogen formation and, as a consequence, efficient cooling of gas in the fragments. On the other hand, the cooling can lead to further fragmentation. We find that the efficient molecule formation starts at  $t \sim 30 - 50 \text{ Myr}$ , which corresponds to the time scale of molecular hydrogen formation on the dust grains. A major part of the  $H_2$  molecules is formed in such fragments, which are the progenitors of molecular clouds. Note that a number of fragments formed may have super-Jeans masses. So, further fragmentation is expected to be amplified by both thermal instability and self-gravity.

A large number of clouds is formed as a result of further evolution: a flocculent structure in the spiral arms can be clearly seen at  $t = 200 \text{ Myr}$  (lower left panel of Figure 2). In the course of collisions the clouds can merge and form bigger ones or can be disrupted completely. In the latter case

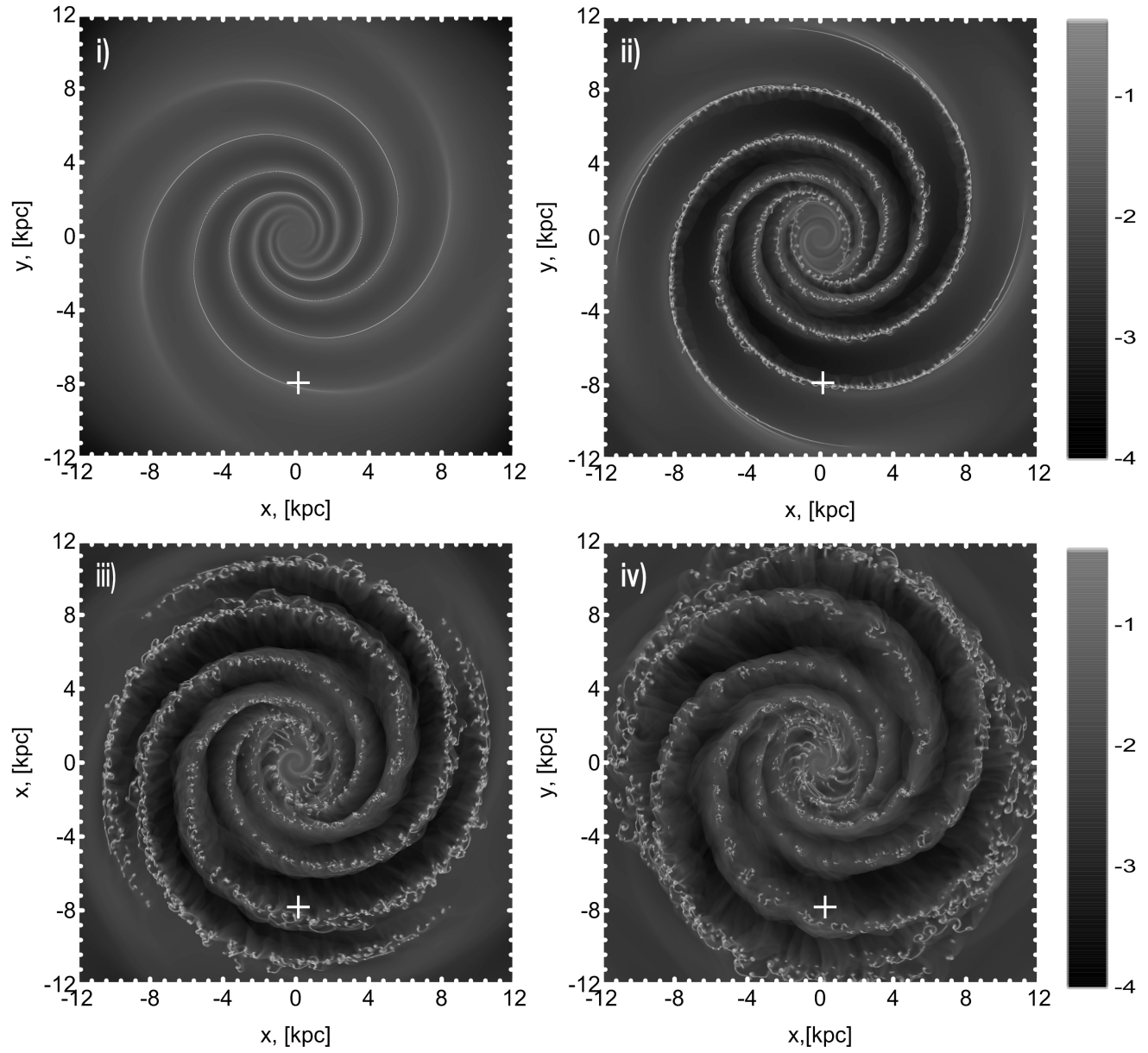


**Figure 2.** The evolution of the surface density of gas ( $\text{g cm}^{-2}$ ) at  $t = 50$  Myr (upper left),  $t = 100$  Myr (upper right),  $t = 200$  Myr (lower left) and  $t = 300$  Myr (lower right). The cross shows position of the Sun (8 kpc).

they produce a number of smaller cloudlets. The clouds moving supersonically through the interstellar medium can be stripped due to the Kelvin-Helmholtz instability. Though  $\text{H}_2$  molecules are formed and destroyed due to these processes, the total mass of molecular gas in the Galaxy increases until  $t \sim 200$  Myr. Then it saturates because the quasi-stationary regime is established between the molecule formation on dust and their destruction by the UV radiation from OB stars (lower left panel of Figure 2). So, at  $t \sim 200$  Myr one finds a population of clouds with sizes varying in the range  $\sim 10 - 100$  pc and typical lifetime about 10 Myr (in the next section we analyze the properties of the clouds in more detail).

At  $t = 200$  Myr groups of clouds are settled along the spiral arms (Figure 2). During further evolution these groups become larger both in size and mass. Gradually they stand apart from each other in the spiral arms. Such agglomerations of clouds have sizes more than 100 pc and the distance between such associations at  $t = 300$  Myr reaches several hundred parsecs. The agglomerations consist of several clouds with the typical number density  $\gtrsim 1 \text{ cm}^{-3}$ . The typical thermal pressure  $p_{th}$  inside such clouds is about  $2-4 M_\odot \text{ pc}^{-2} \text{ K}$  which corresponds to the temperatures  $T \sim 80 - 200$  K. Actual values of the gas temperature are lower because considerable portion of the internal energy is spent on the turbulent motions. However numerical resolution of our simulations is not high enough to resolve the inner structure of the molecular clouds and the turbulent flows. The turbulence (especially small scale one) represents a common and complex problem. At this stage we are not able to extract the turbulent part of the internal energy.

The velocity dispersion in a gas around molecular clouds is about  $3-7 \text{ km s}^{-1}$  and the velocity field around clouds shows a complex turbulent structure. To consider this we pick out a cloud with coordinates  $(-4.9 \text{ kpc}, -4.9 \text{ kpc})$  at  $t = 300$  Myr. Figure 3 shows velocity field around such cloud. The velocities are shown in the comoving coordinate system connected to the most dense part of the cloud. One can see the irregular form of the cloud and the colliding gaseous flows in the regions with enhanced density. The structure and physical parameters of the cloud locations obtained in our numerical simulations are close to those observed in the giant molecular clouds and their surroundings (Roman-Duval *et al.* 2010).

Thermo-chemical processes taken into account in our simulations lead to formation of the two phases of the simulated gas with stable points around  $\sim 100$  K and  $\sim 10^4$  K (Figure 4, see note on the value of the temperature above)). A gas with  $T \sim 100$  K corresponds to the dense molecular clouds, i.e they have both high number density ( $n \sim 100 - 300 \text{ cm}^{-3}$ ) and high  $\text{H}_2$  molecule abundance ( $x(\text{H}_2) \sim 0.3 - 0.5$ ). These clouds concentrate to the spiral arms. A gas belonging to the warmer phase with  $T \sim 10^4$  K is a rarefied atomic gas which resides mainly between the arms. A gas of the coldest phase ( $T \sim 10$  K) occupies negligibly small volume of space and is not considered here.

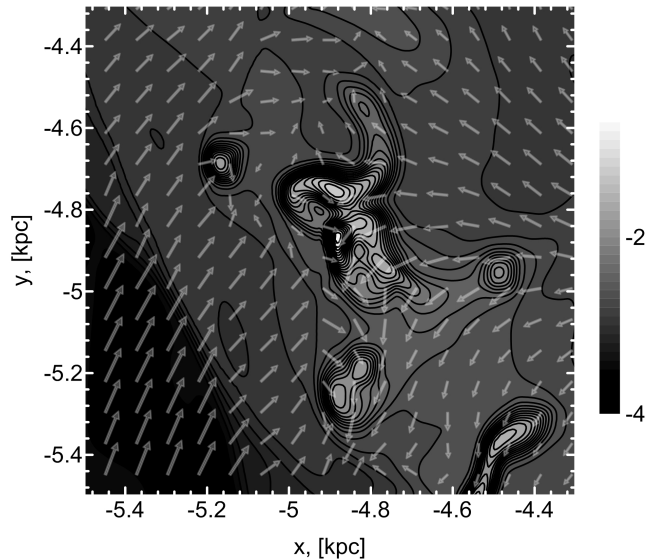


**Figure 3.** The surface gas density ( $\text{g cm}^{-2}$ ) and the velocity field (in the co-moving coordinate system) of the "cloud" with coordinates  $(-4.9 \text{ kpc}, -4.9 \text{ kpc})$  at  $t = 300$  Myr.

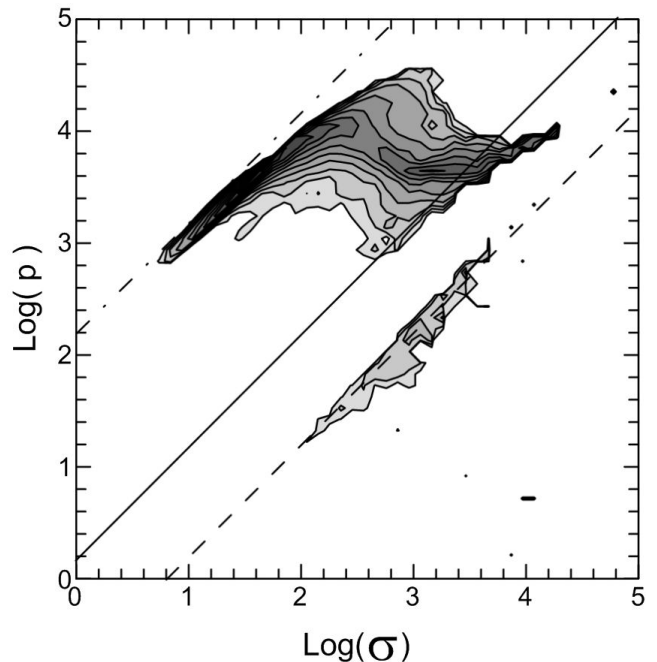


**Figure 4.** The phase diagram of thermal pressure  $p_{th}$  ( $M_\odot \text{ K pc}^{-2}$ ) versus surface density  $\sigma$  ( $M_\odot \text{ pc}^{-2}$ ) at the time  $t = 300$  Myr. The lines correspond to the constant temperature (see note on the value of the temperature in the text): 10 K (dashed line),  $10^2$  K (solid line) and  $10^4$  K (dash-dotted line).

#### 4 THE PHYSICAL PROPERTIES OF MOLECULAR CLOUDS

In this section we consider physical and statistical properties of the molecular gas in our simulations. This gas resides in the clumps which are called molecular clouds. A border of the cloud can be defined as location where  $\text{H}_2$  abundance or  $\text{H}_2$  surface density exceeds given limit. The

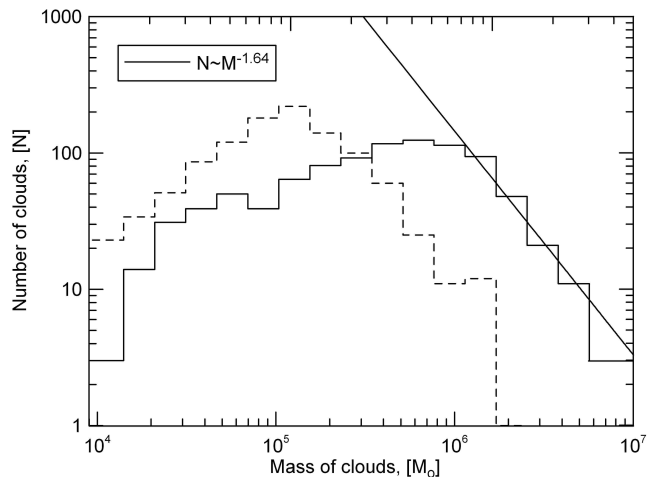


**Figure 5.** Distribution of masses of the clouds for the  $\text{H}_2$  surface density thresholds  $\Sigma_t^{\text{H}_2} = 1.5 \times 10^{-5} \text{ g cm}^{-2}$  (solid line) and  $1.5 \times 10^{-4} \text{ g cm}^{-2}$  (dash line) at  $t = 300 \text{ Myr}$ . The line corresponds to the empirical dependence  $N \sim M^{-1.64}$  obtained by Roman-Duval *et al.* (2010)

clouds in our analysis are delimited using a surface density threshold: over the 2D computational grid of the Galactic plane we find isolated groups of cells with the column density exceeding given threshold. Such clumps normally have irregular form, and their effective linear size is estimated as a square root of their surface  $A$ .

For our analysis we have chosen two values of the molecular hydrogen surface density threshold:  $\Sigma_t^{\text{H}_2} = 1.5 \times 10^{-5} \text{ g cm}^{-2}$  and  $1.5 \times 10^{-4} \text{ g cm}^{-2}$ . In both cases average density inside a cloud is greater than several dozens particles per cc, which is close to the typical value of  $\text{H}_2$  number density obtained from observations of molecular clouds in the Galaxy (e.g. Shu *et al.* 1987).

We are using two thresholds for  $\text{H}_2$  surface density at the border of the cloud in order to show that our basic conclusions on the statistical properties of clouds are independent of exact value of the threshold. This is important because there is no single value of  $\text{H}_2$  surface density which exactly reproduces definition of a molecular cloud in observations.

Figure 5 presents the distribution of masses of the clouds for the  $\text{H}_2$  surface density thresholds  $\Sigma_t^{\text{H}_2} = 1.5 \times 10^{-5} \text{ g cm}^{-2}$  (solid line) and  $1.5 \times 10^{-4} \text{ g cm}^{-2}$  (dash line) at  $t = 300 \text{ Myr}$ .

We find that the spectra of cloud masses for both thresholds follow the power law dependence  $N \sim M^{-1.64}$ : in the mass range  $M \sim 10^5 - 10^6 M_\odot$  for the higher threshold value and in mass range  $M \sim 10^5 - 10^7 M_\odot$  for the lower density threshold. This invariance of the spectrum on surface density limit indicates to that physical processes leading to the formation of the structure with density threshold  $\Sigma_t^{\text{H}_2} \sim 10^{-5} - 10^{-4} \text{ g cm}^{-2}$  have the same nature. Hence, other statistical properties of the structures should be close. Note that the dependence  $N(M)$  for the higher threshold is valid in the same mass range as that obtained in the observations of the Galactic molecular clouds (Roman-Duval *et al.* 2010). For both thresholds one can see a lack of low-mass clouds. In the case of the higher limit the lack of clouds with  $M \lesssim 10^5 M_\odot$  can be explained by our numerical resolution,

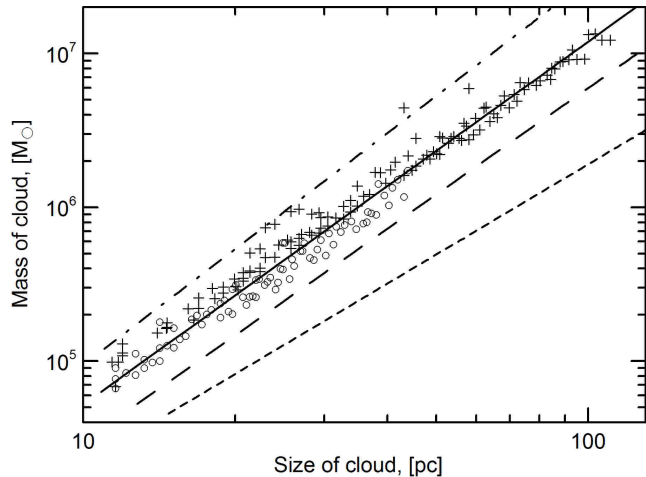


**Figure 6.** Mass-size dependence for the  $\text{H}_2$  surface density thresholds  $\Sigma_t^{\text{H}_2} = 1.5 \times 10^{-5} \text{ g cm}^{-2}$  (crosses) and  $1.5 \times 10^{-4} \text{ g cm}^{-2}$  (circles) at  $t = 300 \text{ Myr}$ . The lines correspond to several theoretical and empirical fits  $(M/M_\odot) = \gamma(A/\text{pc}^2)^\beta$  given in Beaumont *et al.* (2012):  $(\gamma, \beta) = 240, 0.95$  (Larson 1981),  $(\gamma, \beta) = 300, 1.5$  (Elmegreen & Falgarone 1996),  $(\gamma, \beta) = 150, 1.3$  (Román-Zúñiga *et al.* 2010) and  $(\gamma, \beta) = 228, 1.36$  (Roman-Duval *et al.* 2010) shown by dotted, dashed, solid and dash-dotted lines, correspondingly.

whereas similar deficiency in the observations comes from the incompleteness of the data (Roman-Duval *et al.* 2010). For the lower threshold the lack of clouds with  $M \lesssim 10^6 M_\odot$  can be explained by clustering of smaller and denser clumps. In other words, choosing lower surface density level we pick out more extended clusters of clumps, which contain both smaller and denser clumps. In the case of the lower threshold we cover larger regions with lower density, so that the increase of density limit should lead to decrease of size of the cluster and excludes extended low-density regions from consideration of.

Figure 6 presents the dependence of mass of the cloud on its size (mass-size relationship) for the  $\text{H}_2$  surface density thresholds  $\Sigma_t^{\text{H}_2} = 1.5 \times 10^{-5} \text{ g cm}^{-2}$  (crosses) and  $1.5 \times 10^{-4} \text{ g cm}^{-2}$  (circles) at  $t = 300 \text{ Myr}$ . The sizes of the clouds vary between  $\sim 10 - 60 \text{ pc}$  for the higher density threshold. The most massive clouds have masses about  $2 \times 10^6 M_\odot$ . These values are in good agreement with the observational data (Roman-Duval *et al.* 2010). In some cases the sizes of molecular clouds can be as large as  $\sim 100 - 200 \text{ pc}$  (Kirsanova *et al.* 2008), but these regions can be considered as a tight group of smaller clouds. In our analysis such extended clouds can be found under the lower density threshold (crosses in Figure 6): there are groups or chains of clouds seen in the periphery of the Galaxy at 300 Myr (Figure 2).

The mass-size (or mass-area) relationship among molecular clouds,  $M \sim R^2$ , which is well-known as Larson's third law, appears due to cloud evolution and numerous physical processes in the interstellar medium. Many efforts to obtain or explain this universal relation are given in Beaumont *et al.* (2012), who tried to interpret the relationship in terms of the column density distribution function. However, the scatter of the empirical fits is large (see lines in Figure 6, note that we pick out only several fits from the Table 1 presented in Beaumont *et al.* 2012). One can see

that the properties of clouds obtained in the numerical simulations are close to the power-law relation between the radius and mass of the cloud  $M = 228R^{2.36}$ , which was obtained by applying a  $\chi$ -square minimization for the observed radii and masses of the Galactic molecular clouds (Roman-Duval *et al.* 2010). There is a significant dispersion of our simulated data around this fit. We find that our best fit of the simulated data  $M \sim R^{2.14-2.16}$  (the ranges correspond different density thresholds) is close to that obtained in observations. Note that our fit has a power-law index close to 2 for both density thresholds considered here.

Finally, we note that the velocity dispersion for the majority of clouds varies in the range  $v_t \sim 1 - 2 \text{ km s}^{-1}$  in our numerical simulations, that is a good agreement with the observational data (Roman-Duval *et al.* 2010).

Thus, we have found that the physical properties of clouds obtained from our simulation are close to those observed in the Galaxy. Our conclusions are constrained by the numerical resolution, because we can consider clouds with sizes larger than 10 pc, whereas even the parsec-size clouds are observed (Roman-Duval *et al.* 2010). Anyhow, our numerical results provide possibility to consider the global properties of molecular and atomic gas in the Galaxy.

## 5 THE $L - V$ DIAGRAM

### 5.1 Molecular hydrogen

Large-scale distribution of molecular gas in the Galaxy can be represented using the 'longitude-velocity' diagram (henceforth  $l - v$  diagram) constructed from observations of the CO(1-0) line emission (Dame *et al.* 2001). The CO molecule is usually used as a tracer of molecular gas (Maloney & Black 1988) because emission of much more abundant  $\text{H}_2$  molecule cannot be observed in the cold and warm regions. Current model of molecular kinetics in our simulations does not provide us with possibility to calculate abundance of CO molecule and the distribution of molecular gas is judged from the distribution of  $\text{H}_2$ . Certainly, the CO- $\text{H}_2$  conversion factor depends on many physical parameters (Shetty *et al.* 2011; Feldmann *et al.* 2012). However, there are no doubts that the general conclusion on agreement between synthetic and observational distributions of molecular gas in the Galaxy can be drawn from comparison of  $l - v$  diagram for  $\text{H}_2$  molecule in the model with CO data of Dame *et al.* (2001).

Figure 7 presents the  $l - v$  diagram for molecular gas at  $t = 300 \text{ Myr}$ . The diagram is constructed for an observer located at the Sun position (see Figure 2). One can find the large-scale structures corresponding to Perseus, Outer and Carina spiral arms. In the central part of the diagram,  $l \pm (30 - 40)^\circ$ , an intense and extended structure with the strong velocity gradient that passes through the origin is clearly seen. This structure by its location and general appearance resembles so-called Galactic Molecular Ring (Stecker *et al.* 1975; Cohen & Thaddeus 1977; Roman-Duval *et al.* 2010). However, Figure 2 shows that there is no pronounced ring of molecular material in our simulations. In our model the structure in the Molecular Ring locus of points of the  $l - v$  diagram is associated with the Galactic bar and the spiral arms at  $\sim 3\text{-}4 \text{ kpc}$ . Thus, our

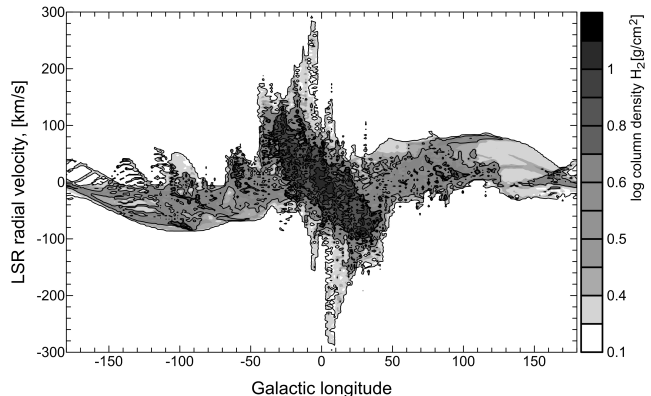


**Figure 7.** The  $l - v$  diagram for the molecular gas at  $t = 300 \text{ Myr}$ . The mass of gas with a given  $(l, v)$  is indicated by grey scale: from small (light grey) to large (black) mass.

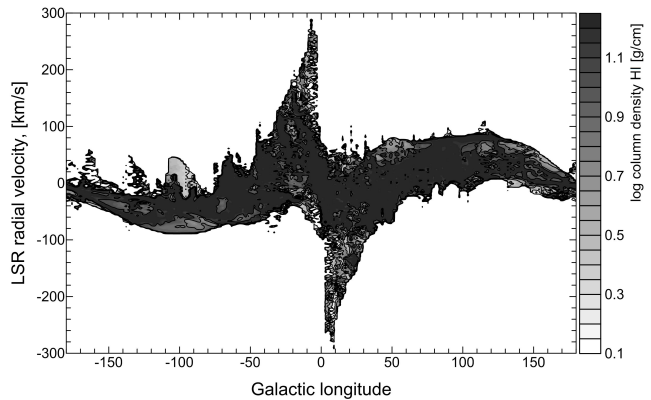


**Figure 8.** The  $l - v$  diagram for the atomic gas at  $t = 300 \text{ Myr}$ . The mass of gas with a given  $(l, v)$  is indicated by grey scale: from small (light grey) to large (black) mass.

results are in agreement with conclusions on the absence of the Molecular Ring drawn from the simple fitting technique Dobbs & Burkert (2012) and previous hydrodynamical simulations (Englmaier & Gerhard 1999; Rodriguez-Fernandez & Combes 2008; Baba *et al.* 2010). Note that the previous simulations did not include molecular chemical kinetics.

We have to note on the existence of numerous small-scale structures in the diagram. They are obviously associated with spurs, agglomerations of clouds and individual clouds. But we make no comment on that here because our consideration is concentrated on the extended structures scales of which greatly exceed our numerical resolution.

### 5.2 Atomic hydrogen

The atomic gas in our model is the main part of the gaseous component of the spiral arms and its distribution traces large-scale structures in the Galaxy. Figure 8 presents the synthetic  $l - v$  diagram for atomic gas at  $t = 300 \text{ Myr}$ . The diagram is constructed for an observer located at the Sun position (see Figure 2). The structures corresponding to the spiral arms are clearly seen in this Figure. The synthetic diagram does not show any prominent structure at the locus of points corresponding to the Galactic Molecular Ring (Figure 8). Results of our modelling show that the atomic



gas in the simulated Galaxy is distributed much more uniformly than the molecular gas. The synthetic  $l-v$  diagram shows reasonably good agreement with the observational data (see, e.g.  $l-v$  diagrams in Kalberla & Dedes 2008; McClure-Griffiths *et al.* 2004). So, our model reproduces main features of the observed distribution of the neutral gas in the Galaxy.

## 6 CONCLUSION

In this paper we have studied formation of gas clouds in the model of our Galaxy. The 3D simulations have taken into account molecular hydrogen chemical kinetics, cooling and heating processes. Comprehensive gravitational potential have been used. It included contributions of self-gravitating gaseous component, stellar bulge, two and four armed spiral structure, stellar disk and dark halo. We have analyzed general properties of the simulated clouds and have compared them with statistical distributions taken from the recent surveys of molecular clouds (Roman-Duval *et al.* 2010).

Our results can be summarized as follows:

- the following stages of evolutionary sequence of the molecular cloud system formation were distinguished in our modelling: a) spurs and fragments (progenitors of molecular clouds) are formed in the spiral arms due to shear and wobble instabilities at the times  $t \lesssim 50$  Myr; b) numerous molecular clouds start to form after  $t \gtrsim 50$  Myr which corresponds to the time scale of molecular hydrogen formation on dust grains; c) a well-developed hierarchical structure of the clouds is formed at  $t \sim 200$  Myr; d) at the moment of time  $t \sim 300$  Myr the clouds agglomerate into extended associations with sizes exceeding 100 pc while the sizes of individual clouds vary in the range  $\sim 10 - 100$  pc;
- the total mass of molecules in the Galaxy increases until  $t \sim 200$  Myr, when it saturates; the major part of molecule hydrogen is locked in molecular clouds where the  $H_2$  molecule abundance reaches  $x(H_2) \sim 0.3 - 0.5$ ;
- the statistical dependencies, e.g. the mass spectrum of clouds, the "mass-size" relation and the velocity dispersion of clouds, obtained in our simulations are close to those observed in the Galaxy (Roman-Duval *et al.* 2010);
- the structure is clearly seen in the Galactic Molecular Ring's locus of points on the simulated  $l-v$  diagram of molecular gas; this structure doesn't correspond to a real ring of molecular gas and likely arises due to superposition of emission from the galactic bar and the spiral arms at  $\sim 3-4$  kpc, which supports conclusion made by (Dobbs & Burkert 2012); no prominent structure in the Galactic Molecular Ring locus of points is distinguished in the simulated  $l-v$  diagram of the HI gas.

## 7 ACKNOWLEDGEMENTS

We thank A.V. Zasov and Yu.A. Shchekinov for thoughtful comments on the manuscript. This work was supported partially by Russian Foundation for Basic Research (grants 11-02-12247-ofi-m-2011, 10-02-00231, 12-02-00685-a) and the President of the Russian Federation grant (SS-3602.2012.2). S.A.K. and E.O.V. thank to the foundation

"Dynasty" (Dmitry Zimin) for financial support. E.O.V. thanks to Russian Foundation for Basic Research (grant 11-02-01332). AMS was partly supported by the Russian federal task program Research and operations on priority directions of development of the science and technology complex of Russia for 2007-2012 (state contract 16.518.11.7074). The numerical simulations were made on the supercomputer facilities of NIVC MSU "Lomonosov" and "Chebyshev".

## References

- Amores, E. B.; Lepine, J. R. D.; Mishurov, Yu. N., 2009, MNRAS, 400, 1768
- Asplund M., Grevesse N., Sauval A.J., The Solar Chemical Composition. Cosmic Abundances as Records of Stellar Evolution and Nucleosynthesis, 2005, ASP Conf. Ser., 336, eds. T. G. Barnes & F. N. Bash, p.25
- Baba J., Saitoh T. R., Wada K., 2010, PASJ, 62, 1413
- Bakes E.L.O., Tielens A.G.G.M., 1994, ApJ, 427, 822
- Ballesteros-Paredes J., Klessen R.S., Mac Low M.-M., Vazquez-Semadeni E., 2007, in Protostars and Planets V, eds. Reipurth B., Jewitt D., and Keil K., University of Arizona Press, p. 63
- Balbus S. A., Cowie L. L., 1985, ApJ, 297, 61
- Barnes J., Hut. P., 1986, Nature, 324, 446
- Beaumont C.N., Goodman A.A., Alves J.F., Lombardi M., Román-Zúñiga C. G., Kauffmann J., Lada C.J., 2012, MNRAS, in press, arXiv:1204.2557
- Begeman K.G., Broeils A.H., Sanders R.H. 1991, MNRAS, 249, 523
- Bergin E.A., Hartmann L.W., Raymond J.C., Ballesteros-Paredes J., 2004, ApJ, 612, 921
- Binney J., Tremaine S., Galactic Dynamics: Second Edition, Princeton University Press, Princeton, 2008, p. 868
- Blitz L., Shu F.H., 1980, ApJ, 238, 148
- Bobylev V.V., Bajkova A.T., 2010, MNRAS, 408, 1788
- Cazaux S., Tielens A.G.G.M., 2004, ApJ, 604, 222
- Chou W., Matsumoto R., Tajima T., Umekawa M., Shibata K., 2000, ApJ, 538, 710
- Cen R., 1992, ApJ, 78, 341
- Cohen R.S., Thaddeus P., 1977, ApJL, 217, 155
- Cox D.P., Gomez G.C., 2002, ApJS, 142, 261
- Dame T.M., Elmegreen B.G., Cohen R.S., Thaddeus P., 1986, ApJ, 305, 892
- Dame T., Hartmann D., Thaddeus P., 2001 ApJ 547, 729
- Draine B.T., Bertoldi F., 1996, ApJ, 468, 269
- Dobbs C.L., Bonnell I.A., 2006, MNRAS, 367, 873
- Dobbs C. L., Bonnell I. A., & Pringle J. E., 2006, MNRAS, 371, 1663
- Dobbs C.L., Bonnell I.A., 2007, MNRAS, 374, 1115
- Dobbs C.L., Bonnell I.A., 2007, MNRAS, 376, 1747
- Dobbs C.L., 2008, MNRAS, 391, 844
- Dobbs C.L. & Burkert A., 2012, MNRAS, 421, 2940
- Efremov Y. N., 2009, Astr. Letters 35, 507
- Elmegreen B. G., 1979, ApJ, 231, 372
- Elmegreen B. G., 1994, ApJ, 433, 39
- Elmegreen B., Falgarone E. 1996, ApJ, 471, 816
- Elmegreen B.G., 2004, MNRAS 354, 367
- Englmaier P., Gerhard O., 1999, MNRAS, 304, 512
- Falgarone E., Puget J.-L., & Perault M. 1992, A&A, 257, 715



Feldmann R., Gnedin N.Y., Kravtsov A.V., 2012, ApJ, 747, 124  
 Fridman A.M., Khoperskov A.V., Physics of galactic disks, Fizmalit 2011, 640 (in Russian)  
 Field G. B., Saslaw W. C., 1965, ApJ, 142, 568  
 Galli D., Palla F., 1998, A&A, 335, 403  
 Goldsmith P., Langer W.D., 1979, ApJS, 222, 881  
 Glover S.C.O., Federrath C., Mac Low M.-M., Klessen R.S., 2010, MNRAS, 404, 2  
 Glover S. C. O., & Mac Low M., 2011, MNRAS, 412, 337  
 Habing H.J., 1968, BAIN, 19, 421  
 Heyer M., Krawczyk C., Duval J., & Jackson J. M. 2009, ApJ, 699, 1092  
 Hollenbach D., McKee C.F., 1979, ApJS, 41, 555  
 Hollenbach D., McKee C.F., 1989, ApJ, 342, 306  
 Kalberla P.M.W., Dedes L., 2008, A&A, 487, 951  
 Kauffmann J., Pillai T., Shetty R., Myers P. C., & Goodman A. A. 2010, ApJ, 712, 1137  
 Khoperskov A.V., Tyurina N. V. 2003, ARep, 47, 443  
 Kirsanova M.S., Sobolev A.M., Thomasson M., Wiebe D.S., Johansson L.E.B., Seleznev A.F., 2008, MNRAS 388, 729  
 Kim W.-T., Ostriker E. C., 2006, ApJ, 646, 213  
 Kwan J., Valdes F., 1987, ApJ, 315, 92  
 Lada C.J., Lada E.A., 2003, ARA&A, 41, 57  
 Lada, C. J., Muench, A. A., Rathborne, J., Alves, J. F., & Lombardi, M. 2008, ApJ, 672, 410  
 Larson R.B., 1981, MNRAS, 194, 809  
 Lepine J.R.D., Mishurov Yu.N., Dedikov S.Yu., 2004, ApJ, 546, 234  
 Levinson F. H., Roberts Jr. W. W., 1981, ApJ, 245, 465  
 Mac Low M.-M., Shull J.M., 1986, ApJ, 302, 585  
 Maloney P., Black J.H., 1988, ApJ, 325, 389  
 McClure-Griffiths N.M., Dickey J.M., Gaensler B.M., Green A.J., 2004, ApJL, 607, 127  
 McKee C.F., Ostriker E.C., 2007, ARA&A, 45, 565  
 Mishurov I.N., Suchkov A.A., 1975, ApSS, 35, 285  
 Nelson A.H., Matsuda T., 1977, MNRAS, 179, 663  
 Rathborne J.M., Johnson A.M., Jackson J.M., Shah R.Y., Simon R., 2009, ApJS, 182, 131  
 Roberts W.W., 1969, ApJ, 158, 123  
 Roberts W. W., Stewart G. R., 1987, ApJ, 314, 10  
 Rodriguez-Fernandez N. J., Combes F., 2008, A&A, 489, 115  
 Román-Zúñiga C. G., Alves J. F., Lada C. J., & Lombardi M. 2010, ApJ, 725, 2232  
 Roman-Duval J., Jackson J. M., Heyer M., Rathborne J., Simon R., 2010, ApJ, 723, 92  
 Shetty R., Ostriker E.C., 2006, ApJ, 647, 997  
 Shetty R., Glover S.C., Dullemond C.P., Ostriker E.C., Harris A.I., Klessen R.S., 2011, MNRAS, 415, 3253  
 Shu F.H., Adams F.C., Lizano S., 1987, ARA&A, 25, 23  
 Sofue Y., Honma M., Omodaka T., 2009, PASJ, 61, 227  
 Solomon P. M., Rivolo A. R., Barrett J., & Yahil A. 1987, ApJ, 319, 730  
 Spitzer L., 1953, ApJ 118, 106  
 Stecker F.W., Solomon P.M., Scoville N.Z., Ryter C.E., 1975, ApJ, 201, 90  
 Sutherland R.S., Dopita M.A., 1993, ApJS, 88, 253  
 Tasker E.J., & Tan J.C., 2009, ApJ, 700, 358  
 Tielens A.G.G.M., Hollenbach D., 1985, ApJ 291, 722  
 Tomisaka K., 1984, PASJ, 36, 457

van Leer B., 1979, Journ. Comput. Phys., 32, 101  
 Wada. K., 1994, PASJ, 46, 165  
 Wada K., Spaans M., Kim S., 2000, ApJ, 540, 797  
 Wada K., 2001, ApJL., 559, 41  
 Wada K. & Koda J., 2004, MNRAS, 349, 270  
 Wolfire M.G., McKee C.F., Hollenbach D., Tielens A.G.G.M., 2003, ApJ, 587, 278  
 Zhang T. J. & Song G. X., 1999, Ap&SS, 266, 521

## APPENDIX A: EXTERNAL GRAVITATIONAL POTENTIAL MODEL

The dark matter halo gravitational potential is taken in the quasi-isothermal form (Begeman *et al.* 1991):

$$\Psi_{halo} = \frac{M_h}{C_h} \cdot \left\{ \ln(\xi) + \frac{\arctg(\xi)}{\xi} + \frac{1}{2} \ln \frac{1 + \xi^2}{\xi^2} \right\}. \quad (A1)$$

where  $\xi = r/a_h$ ,  $M_h$  is the mass of the dark halo within a radius  $r_h$ ,  $a_h$  is the scale of the halo and  $C_h = a_h(r_h/a_h - \arctg(r_h/a_h))$ . In our model we take  $r_h = 12$  kpc,  $a_h = 6$  kpc,  $M_h = 0.64 \cdot 10^{11} M_\odot$ .

For the stellar bulge potential we adopt the King's model with the cutoff at radius  $r_b^{max}$  (Fridman & Khoperskov 2011)

$$\Psi_{bulge} = -\frac{M_b}{rC_b} \ln \left[ \frac{r}{r_b} + \left( 1 + \left( \frac{r}{r_b} \right)^2 \right) \right], \quad (A2)$$

with the following parameters  $M_b = 0.092 \cdot 10^{11} M_\odot$ ,  $r_b = 0.2$  kpc,  $r_b^{max} = 12$  kpc, where

$$C_b = \ln(r_b^{max}/r_b + \sqrt{1 + (r_b^{max}/r_b)^2}) - (r_b^{max}/r_b)/(\sqrt{1 + (r_b^{max}/r_b)^2}).$$

For the three-dimensional stellar disk we take the exponential distribution of surface density, then the stellar disk potential can be written as follows (Binney & Tremaine 2008)

$$\Psi_{disk} = \pi\sigma_0 z_d \cdot \ln(\cosh(z/z_d)) - \pi\sigma_0 r_d \cdot y \cdot (I_0(y) K_1(y) - I_1(y) K_0(y)), \quad (A3)$$

where  $y = \frac{r}{2 \cdot r_d}$ ,  $\sigma_0 = \frac{M_d}{2\pi \cdot r_d^2}$  is the central surface density,  $M_d = 0.4 \cdot 10^{11} M_\odot$ , the radial scale of disk  $r_d = 3$  kpc, the vertical scale  $z_d = 100$  pc,  $I_0(y)$ ,  $K_0(y)$ ,  $I_1(y)$ ,  $K_1(y)$  are the cylindrical Bessel functions of the first and second kind, respectively.

Taking account the gravitational potentials of bar and spiral structure of stellar component we can obtain more realistic distribution of gas in the Galaxy. Following Cox & Gomez (2002) the perturbed potential of stellar disk  $\Psi_{disk}^*$  can be written in the form of superposition of potentials generated by the bar and the two and four-armed logarithmic spiral patterns:

$$\Psi_{disk}^* = \Psi_{disk} \cdot (1 + \varepsilon(t) \cdot \Psi_{arms}), \quad (A4)$$

where  $\varepsilon(t)$  describes the evolution of the relative amplitude of the spiral stellar density wave. We assume a linear increase of the amplitude  $\varepsilon(t < \tau) = 0.1 \cdot \frac{t}{\tau}$  during  $\tau = 220$  Myr, after that time the amplitude is constant:  $\varepsilon(t > \tau) = 0.1$ .

The relative perturbation  $\Psi_{arms}$  is adopted in the form (Wada & Koda 2004):

$$\Psi_{arms} = \frac{\kappa_1 \cos(\Theta_1)}{(1 + \kappa_1)^{3/2}} + \frac{\kappa_2 \cos(\Theta_2)}{(1 + \kappa_2)^{3/2}} + \frac{\kappa_4 \cos(\Theta_4)}{(1 + \kappa_4)^{3/2}}, \quad (\text{A5})$$

where  $\kappa_1 = (r/r_{a1})^2$ ,  $\kappa_2 = (r/r_{a2})^2$ ,  $\kappa_4 = (r/r_{a4})^2$ ;  $r_{a1} = 2$  kpc,  $r_{a2} = 7$  kpc,  $r_{a4} = 7$  kpc are the radial scales for bar, two-armed and four-armed spiral patterns, respectively. The functions  $\Theta_i$  are:

$$\Theta_1 = 2 \cdot (\phi - f_1),$$

$$\Theta_2 = 2 \cdot (\phi - f_2 - \cot(i_2) \cdot \ln(r/r_{02})),$$

$$\Theta_4 = 4 \cdot (\phi - f_4 - \cot(i_4) \cdot \ln(r/r_{04})),$$

$f_1 = f_2 = f_4 = 50^\circ$  are the phases of bar and spiral patterns,  $r_{02} = r_{04} = 3.5$  kpc,  $i_2 = i_4 = 18^\circ$  are the scales and the pitch angles of two-armed and four-armed components.